Modelling Extrusion Cooking

Chin-Hsien Li *
CSIRO Mathematical and Information Sciences

ABSTRACT A one-dimensional computer model of extrusion cooking has been developed. This model can simulate and predict extruder behavior (such as pressure, temperature, fill factor, gelatinization, residence time distribution, shaft power) under various operating conditions (such as feed rate, screw speed, feed temperature/moisture, barrel temperature). With a very fast and efficient solution algorithm, this model runs fast on a PC, taking only a fraction of a second to a few seconds. In addition, with a graphic user interface, this model is user friendly. Some results of numerical simulation will be presented.

1 INTRODUCTION

Extrusion cooking technology has been widely used in the food industry to make variety of products such as snack food, baby food, breakfast cereals, pastas, wrapper for oriental dumplings, pet foods, etc. An extruder consists basically of one or two screw shafts within a barrel. The food material is transported down the barrel by the rotating screws and exits through a die of given shape. Extrusion cooking is, in general, a high temperature, high pressure and short time process. This process allows for modifications to the food texture and flavour. In order to maintain consistent product quality and improve productivity, it is crucial that one is able to optimize and properly control extruder operating conditions. As a step toward this goal, we need to understand, simulate and predict extruder behavior (such as pressure, temperature, fill factor, gelatinization, residence time distribution, shaft power) under various operation conditions (such as feed rate, screw speed, feed temperature/moisture, barrel temperature). There are basically two approaches to this problem. One is 3-D CFD simulation. However, the complex geometry of the extruder, especially the twin-screw, make the 3-D CFD simulation too difficult to realize and too time consuming to be useful for the purpose of optimizing and controlling extruder operating conditions.

To avoid the difficulty of complex geometry and to reduce the computational cost, an alternative approach is 1-D modelling. In view of the generally fast screw speed, if one is not concerned about the details in the directions normal to the screw shaft, we can assume uniform conditions over the extruder sections normal to the shaft and consider the flow to be one-dimensional. Of course, the variables associated with this one-dimensional flow (e.g. pressure and temperature), are in some sense the averaged quantities over the extruder sections normal to the shaft. 1-D modelling is an efficient tool for understanding the averaged physical process and for the purpose of control. A basic 1-D model can predict pressure profile, temperature profile, shaft power input, fill factor, gelatinization, residence time distribution under various operation conditions (such as feed rate, screw speed, feed temperature/moisture, barrel temperature) for given screw geometry and material properties.

Chen and White [1994] developed a steady state model based on the functional relations between the throughput, pressure drop, viscosity, and screw speed, and an iterative solution algorithm which calculates the pressure profile backward from the die end, followed by the forward calculation of the temperature profile.

Based on the fundamental mass and heat balances, Kulshreshtha and et all ([1991],[1992]) developed a differential equations model for both steady and unsteady situations. They also developed a forward solution algorithm for the transient model, assuming only one inter-zonal interface, and a forward algorithm for the steady state model which performs iterative improvements of the interface location. Their model, however, can only deal with simple screw configurations without paddles and orifices. Another drawback in their model is the formulation of the differential equation for mass balance in terms of *fill factor*, a discontinuous quantity, which can cause numerical difficulties.

Starting from the same idea of 1-D mass and heat balances, the author has corrected the drawback in their model and, with the APV MPF40 co-rotating twin-screw extruder in mind, extended the model to the case of *multi-inter-zonal interfaces* and to more general screw configurations with paddles and an orifice. Furthermore, the author has also designed a very fast and efficient solution algorithm with which the solution time on a PC ranges from a fraction of a second to a few seconds.

2 1-D MODEL

2.1 Basic Physics

Along its length, the extruder barrel can be divided into alternating regions of partially-filled zones (e.g. solid conveying zone, or partially-filled melt zone) and fully-filled zones (e.g. fully-filled melt pumping zone, melt shearing zone). In the partially-filled zone (PFZ), there is no pressure build-up. This means the pressure gradient is zero and the pressure is generally equal to the air pressure inside the barrel. Viscous heat generation in this zone has been neglected by some authors. However, as pointed out by others, there exists significant viscous

*Postal address: CSIRO Mathematical and Information Sciences, Locked Bag 17, North Ryde, NSW 2113

heat generation in this zone and it should be taken into account.

While, in the fully-filled zone (FFZ), a pressure gradient will develop. The flow in this zone has two components: (1) flow generated by the pumping effect of the screw. In most cases, this is a forward flow, but it could be a backward flow if a reverse screw element is used; (2) pressure flow, which could be a backward flow (called leakage backflow) if there is a forward pressure build-up, but could also be a forward flow if there is a forward pressure drop. Taking the APV MPF40 co-rotating twin-screw extruder as an example, it has basically two kinds of screw sections: forward pumping screw sections and paddle sections. In the forward pumping screw sections, the net forward flow is the difference between the maximum pumping capacity of the twin-screw and the leakage backflow. While in the paddle sections, the net forward flow has two components: pressure flow, and flow generated by the pumping effect of the paddle which may be forward or backward depending on the staggering angle of the paddles.

The FFZ is responsible for generating pressure to overcome any section offering flow restriction. The location of the *peak pressure* coincides with the *beginning of the restriction.* The length of the FFZ depends on the pressure needed for the melt to flow across the restriction section. In the down barrel direction (i.e. the direction from the feed end to the die end), the *first and last zone are always PFZ and FFZ*, respectively. It is generally assumed (Chen and White [1994],Kulshreshtha and et all ([1991],[1992]),Yacu[1983]) that there exist *distinct boundaries* between PFZs and FFZs. In the down barrel direction, a boundary from a PFZ to a FFZ is the point where the *pressure changes from air pressure to great than air pressure and the pressure gradient changes from zero to positive*, while a boundary from a FFZ to a PFZ is at the point where the *pressure changes from great than to equal to air pressure and the pressure gradient changes from negative to zero.* Note that the boundary from a FFZ to a PFZ can also be determined from the screw geometry as the *end point of the restriction section.* In any case, the *number of FFZ can not be greater than the number of the restriction sections.* In some cases, however, it is possible that the *number of FFZ is less than the number of the restriction sections*, depending on the operating conditions.

To simplify the analysis, we will make the following assumptions:

- one-dimensional flow;
- distinct boundaries between PFZs and FFZs;
- constant density and specific heat;
- negligible heat loss to the screw shafts.

2.2 Transient (Dynamic) Model

Assume that the x-axis is pointing towards the die end with the origin at the feed inlet. The transient model equations for each zone can be derived from the mass and heat balances across a control volume of length Δx, and these model equations are presented below. (The notations used in this paper are listed in §8.)

2.2.1 Model equations for PFZ

$$\frac{\partial F}{\partial t} = -\xi N \frac{\partial F}{\partial x}, \tag{1}$$

$$\frac{\partial M}{\partial t} = -\xi N \frac{\partial M}{\partial x}, \tag{2}$$

$$\frac{\partial T}{\partial t} = -\xi N \frac{\partial T}{\partial x} + \frac{\phi C_s N^2 \eta_s}{V_s \rho s f} + \frac{U_s c_e \xi}{V_s \rho s}(T_b - T) \tag{3}$$

Note that Kulshreshtha and et al ([1991],[1992]) proposed a PDE of fill factor f for mass balance, which is not quite correct mathematically since fill factor f is, in general, discontinuous due to the discontinuity of the geometry parameter V_s across different screw geometry. This drawback can cause numerical difficulties. To correct this drawback, a PDE of net forward mass flow rate F, which is continuous, is used here.

2.2.2 Model equations for FFZ

$$-B\rho \frac{1}{\eta_m}\frac{\partial P}{\partial x} + V_s N \rho = F_m, \tag{4}$$

$$\frac{\partial M}{\partial t} = -\frac{F_m \xi}{V_s \rho}\frac{\partial M}{\partial x}, \tag{5}$$

$$\frac{\partial T}{\partial t} = -\frac{F_m \xi}{V_s \rho}\frac{\partial T}{\partial x} + \frac{C_m N^2 \eta_m}{V_s \rho s} + \frac{U_m c_e \xi}{V_s \rho s}(T_b - T) \tag{6}$$

Note that the net forward mass flow rate $F = F_m$ is a constant along a FFZ.

Remark 2.1 For paddle sections, ξ and V_s should be replaced by e and V_p, respectively, in equations (5)-(6), while for reverse screws, V_s should be replaced by its absolute value $|V_s|$.

Remark 2.2 The shaft power at any instant is the sum of the power consumed due to viscous dissipation in the PFZs and the FFZs, and the power required to force the material through the die:

$$E = \int_{PFZ} \frac{\phi C_s N^2}{\xi}\eta_s \, dx + \int_{FFZ_s} \frac{C_m N^2}{\xi}\eta_m \, dx + \int_{FFZ_p} \frac{C_m N^2}{e}\eta_m \, dx + P_d F_d/\rho, \tag{7}$$

where FFZ_s denotes screw elements in FFZ, while FFZ_p denotes paddle elements.

Remark 2.3 The following power-law models are assumed for viscosity:

$$\eta_m = \eta_m^0 \gamma^n e^{-\delta T} e^{-\beta M}, \quad \textit{for plasticized melt},$$

where the overall (average) shear rate for screw sections is $\gamma = N\sqrt{C_m/|V_s|}$, and, for paddle sections, $\gamma = N\sqrt{C_m/V_p}$.

$$\eta_s = \eta_s^0 e^{-\beta_s M}, \quad \textit{for unplasticized solid-water mixture};$$

$$\eta_d = \eta_m \gamma_d^{n_d}, \ \textit{with } \gamma_d = \frac{32Q}{\pi d^3}, \ \textit{for melt at the die.}$$

2.2.3 Boundary conditions

At $x = 0$: $P = 0$, $T = T_0$, $M = M_0$, $F = F_0$.

At a PFZ-to-FFZ interface: $P = 0$, and $\{T,\ M\}$ are continuous. (Note that F is continuous only at steady state.)

At a FFZ-to-PFZ interface: $P = 0$, and $\{T,\ M,\ F\}$ are continuous.

At the die end ($x = L_b$), $P_d = \frac{F_d \eta_d}{\rho K_d}$.

Note that, in the case of multi-feed-ports, both M and F are, in general, discontinuous at the ports.

2.2.4 Moving interface condition

During the transient stage, the location of PFZ-to-FFZ interfaces will, in general, change due to the difference between the incoming and outgoing mass flow rates. Let F_s and f_s be the mass flow rate and fill factor on the PFZ side of the interface, and F_m the mass flow rate on the FFZ side. Then we have

$$\frac{dl_s}{dt} = \frac{\xi(F_m - F_s)}{V_s \rho (1 - f_s)}. \tag{8}$$

Remark 2.4 The FFZ-to-PFZ interfaces can be determined from the screw geometry as the *end point of the restriction section*, While the location of the PFZ-to-FFZ interfaces is, in general, unknown and must be calculated along with the solution.

2.3 Steady-State Model

In the steady-state, the mass flow rate F and the moisture content M are constant in each section between two feed ports, and the inter-zonal interface is stationary. The steady-state model can be obtained from the transient model by setting the partial time derivative to zero:

Model for PFZ.

$$\frac{\partial T}{\partial x} = \frac{\phi C_s N^2 \eta_s}{\xi F s} + \frac{f U_s c_e}{F s}(T_b - T). \tag{9}$$

Model for FFZ.

$$-B\rho \frac{1}{\eta_m}\frac{\partial P}{\partial x} + V_s N \rho = F \tag{10}$$

$$\frac{\partial T}{\partial x} = \frac{C_m N^2 \eta_m}{\xi F s} + \frac{U_m c_e}{F s}(T_b - T), \tag{11}$$

For paddle sections, as in Remark 2.1, ξ in (11) should be replaced by e .

Remark 2.5 In the steady-state, the mass flow rate is equal to the feed rate, and the location of the FFZ-to-PFZ interfaces can be determined from the screw geometry as the *end point of the restriction section.* Then from these known locations of the FFZ-to-PFZ interfaces, we can solve the pressure equation (10) backwards. The locations of the PFZ-to-FFZ interfaces can then be determined as the points where the *pressure changes from great than air pressure to air pressure.*

2.4 Approximate Calculation of Parameters

In this subsection, we briefly discuss the approximate calculation of geometry-related parameters $\{V, c_e, D_e, C_m, C_s, B\}$, used in the above model equations; in particular, for APV Baker MPF40 twin screw extruder elements. For single lead or double lead screws, the calculation of these parameters can be found in Martelli[1983] and Frame[1994]. Consequently, the discussion below is for **paddles**:

According to Frame[1994], the cross-sectional area available for process is $A = 0.699D^2$. Thus,

$$V_p = Ae = 0.699D^2 e, \qquad c_e = 2(\pi D - \sqrt{2Dh}),$$

where h should be interpreted as the maximum distance from a paddle to the barrel surface. Define the average depth $H = \frac{A}{c_e}$. The parameters C_m and B are calculated as follows:

$$C_1 = (\frac{\pi D}{H})^2 \cdot V_p, \qquad C_2 = \frac{3\pi^2 D^2 e l_p}{\chi},$$

$$C_3 = \frac{16\pi I^3 e l_p}{\epsilon D}, \qquad C_4 = \frac{\pi^2 I^2}{\sigma} \cdot \frac{8yA_t}{\pi I} = \frac{8yA_t \pi I}{\sigma},$$

where A_t is one half of the maximum area of contact between one upstream paddle and the opposite downstream paddle, while y is one half of the maximum width of the paddle tip in contact; and

$$C_m = C_1 + C_2 + C_3 + C_4, \quad B = \frac{c_e H^3}{12}.$$

The paddle section may be seen as an approximate double lead screw. The cross-section of a paddle is approximately an ellipse with the two ends truncated, whose long axis is $2r_a$ and short axis is $2r_b$. For a paddle section with a stagering angle α, the effective screw diameter is $D = 2r$ with $r = \frac{1}{\sqrt{(\frac{\cos\frac{\alpha}{2}}{r_a})^2 + (\frac{\sin\frac{\alpha}{2}}{r_b})^2}}$, the effective channel depth is $h = r - r_b$, and the pitch length is $\xi = \frac{360^\circ}{\alpha} \cdot e$. From these quantities, the effective conveying volume $V_s = 4V$ can be calculated similarly to double lead screws. The parameter C_s is calculated as follows:

$$C_1 = (\frac{\pi D}{h})^2 \cdot 4V, \qquad C_2 = 0,$$

$$C_3 = \frac{16\pi I^3 e l_p}{\epsilon D} \cdot \frac{\xi}{e}, \qquad C_4 = \frac{8yA_t \pi I}{\sigma} \cdot (\frac{\xi}{e} - 1),$$

and

$$C_s = C_3 + C_4,$$

Remark 2.6 The values of C_s, C_m and B, as calculated above, can only be used as a first approximation. These values need to be adjusted, if possible, by measurement, or via nonlinear regression.

3 SOLUTION ALGORITHM

3.1 Solution Algorithm for Transient Model

Assume that at the n-th time level $t = t^n$ the solutions $\{F^n, P^n, T^n, M^n\}$ are known and there exist $I \geq 1$ pairs of (PFZ, FFZ), and the positions of the i-th PFZ (PFZ^i) to i-th FFZ (FFZ^i) interface $l_{PF}^{i,n}$, $i = 1, ..., I$, are also known, while the positions of the i-th FFZ (FFZ^i) to (i+1)-th PFZ (PFZ^{i+1}) interface l_{FP}^{i}, $i = 0, ..., I$, are known from screw geometry (note that $l_{FP}^{0} = 0$ denotes the feed end, while $l_{FP}^{I} = L_b$ denotest the die end). The solutions of transient model (1)-(6) at the (n+1)-the time level are obtained segregately in the following steps:

[1] Using T^n, M^n, calculate η^n at all mesh points at the n-th time level. Note that $l_{PF}^{i,n}$ and l_{FP}^{i} are always taken as mesh points at the n-th level.

[2] Using η_m^n calculated in step [1], solve the mass balance equations (1) and (4) with moving PFZ-to-FFZ interfaces to obtain $\{F^{n+1}, P^{n+1}, l_{PF}^{i,n+1}\}$.

[3] Using η_s^n, η_m^n calculated in step [1] and $l_{PF}^{i,n+1}$ obtained in step [2], solve the moisture equations (2) and (5) to obtain M^{n+1}, and solve the heat equations (3) and (6) to obtain T^{n+1}.

3.1.1 Predictor-corrector scheme for step [2]

The following predictor-corrector scheme is used to obtain $\{F^{n+1}, P^{n+1}, l_{PF}^{i,n+1}\}$:

Predictor:

1) Using the moving interface condition (8) to predict the positions $l_{PF}^{i,*}$ of the PFZ-to-FFZ interfaces at the (n+1)-th time level as

$$l_{PF}^{i,*} = l_{PF}^{i,n} + \Delta t \cdot \frac{\xi(F_m^{i,n} - F_s^{i,n})}{V_s \rho (1 - f_s^{i,n})},$$

for i=1,...I, with $\Delta t = t^{n+1} - t^n$, $f_s^{i,n} = \frac{F_s^{i,n}}{V_s N \rho}$, and the last term is evaluated at $x = l_{PF}^{i,n}$.

2) Integrate the pressure equation (4) to predict the flow rate $F_m^{i,*}$ in FFZ^i, i=1,...,I, at the (n+1)-th time level as

$$F_m^{i,*} = \frac{N\rho \int_{l_{PF}^{i,*}}^{l_{FP}^{i}} \frac{V_s}{B}\eta_m^n \, dx}{\int_{l_{PF}^{i,*}}^{l_{FP}^{i}} \frac{1}{B}\eta_m^n \, dx}, \quad for\ i < I;$$

$$F_m^{I,*} = \frac{F_n}{F_d + w(F_m^{I,*})^{n_d}}, \quad with$$

$F_n = N\rho \int_{l_{PF}^{I,*}}^{l_{FP}^{I}} \frac{V_s}{B}\eta_m^n \, dx$, $F_d = \int_{l_{PF}^{I,*}}^{l_{FP}^{I}} \frac{1}{B}\eta_m^n \, dx$, and $w = \frac{\eta_m^n}{K_d}(\frac{32}{\pi d^3 \rho})^{n_d}$.

Note that $F_m^{I,*}$ can be obtained by either fixed point iteration or Newton's iteration.

3) Solve the mass balance equation (1) in $PFZ^i = [l_{FP}^{i-1}, l_{PF}^{i,*}]$, i=1,...I, to predict the flow rate $F_s^{i,*}$ in PFZ^i at the (n+1)-th time level. The boundary condition used for (1) in PFZ^i is:
$F_s^{1,*} = F_0$, at $x = 0$; $F_s^{i,*} = F_m^{i-1,*}$, at $x = l_{FP}^{i-1}$ for $i > 1$.

Corrector:

1) Using the moving interface condition (8) to compute the positions $l_{PF}^{i,n+1}$ of the PFZ-to-FFZ interfaces at the (n+1)-th time level as

$$l_{PF}^{i,n+1} = \frac{1}{2}(l_{PF}^{i,*} + l_{PF}^{i,**}), \quad with$$

$$l_{PF}^{i,**} = l_{PF}^{i,n} + \Delta t \cdot \frac{\xi(F_m^{i,*} - F_s^{i,*})}{V_s \rho (1 - f_s^{i,*})},$$

for i=1,...I, with $f_s^{i,*} = \frac{F_s^{i,*}}{V_s N \rho}$, and the last term is evaluated at $x = l_{PF}^{i,*}$.

2) Integrating the pressure equation (4) to obtain the flow rate $F_m^{i,n+1}$ in FFZ^i, i=1,...,I, at the (n+1)-th time level as

$$F_m^{i,n+1} = \frac{N\rho \int_{l_{PF}^{i,n+1}}^{l_{FP}^{i}} \frac{V_s}{B}\eta_m^n \, dx}{\int_{l_{PF}^{i,n+1}}^{l_{FP}^{i}} \frac{1}{B}\eta_m^n \, dx}, \quad for\ i < I;$$

$$F_m^{I,n+1} = \frac{F_n}{F_d + w(F_m^{I,n+1})^{n_d}}, \quad with$$

$F_n = N\rho \int_{l_{PF}^{I,n+1}}^{l_{FP}^{I}} \frac{V_s}{B}\eta_m^n \, dx$, $F_d = \int_{l_{PF}^{I,n+1}}^{l_{FP}^{I}} \frac{1}{B}\eta_m^n \, dx$, and $w = \frac{\eta_m^n}{K_d}(\frac{32}{\pi d^3 \rho})^{n_d}$.

Note that $F_m^{I,n+1}$ can be obtained by either fixed point iteration or Newton's iteration.

3) Solve the mass balance equation (1) in $PFZ^i = [l_{FP}^{i-1}, l_{PF}^{i,n+1}]$, i=1,...I, to obtain the flow rate $F_s^{i,n+1}$ in PFZ^i at the (n+1)-th time level. The boundary condition used for (1) in PFZ^i is:
$F_s^{1,n+1} = F_0$, at $x = 0$; $F_s^{i,n+1} = F_m^{i-1,n+1}$, at $x = l_{FP}^{i-1}$ for $i > 1$.

4) Compute $P^{i,n+1}$ in $FFZ^i = [l_{PF}^{i,n+1}, l_{FP}^{i}]$, i=1,...,I, by numerical integration of the pressure equation (4) with boundary condition $P^{i,n+1} = 0$, at $x = l_{PF}^{i,n+1}$.

3.1.2 Discretization schemes

All the equations in the transient model, except (4), are of the following type

$$\frac{\partial T}{\partial t} = -v\frac{\partial T}{\partial x} + Q(x, T) \tag{12}$$

Let x_j be the j-th mesh point, $\Delta x_j = x_j - x_{j-1}$, $T_j^n = T(x_j, t^n)$. For the numerical solution of (12), the following implicit finite difference scheme is used:

$$\frac{T_j^{n+1} - T_j^{i,n}}{\Delta t} = -v\frac{T_j^{n+1} - T_{j-1}^{n+1}}{\Delta x_j} + Q(x_j, T_j^{n+1}) \tag{13}$$

In each PFZ^i or FFZ^i, the mesh size is constant, except next to the PFZ-to-FFZ interface. Moreover, all the inter-zonal interfaces are always taken as mesh points.

3.2 Solution Algorithm for Steady-State Model

The steady-state model is solved by a segregated iteration scheme. Assume that, at the n-th iteration, the solutions $\{P^n, T^n\}$ are known and there exist $I \geq 1$

pairs of (PFZ, FFZ), and the positions of PFZ^i-to-FFZ^i interface $l_{PF}^{i,n}$, $i = 1, ..., I$, are also known, while the positions of FFZ^i-to-PFZ^{i+1} interface l_{FP}^i, $i = 0, ..., I$, are known from screw geometry (note that $l_{FP}^0 = 0$ denotes the feed end, while $l_{FP}^I = L_b$ denotest the die end). The solutions at the (n+1)-the iteration are obtained segregately as follows:

[1] Using T^n, calculate η^n at all mesh points at the n-th iteration. Note that $l_{PF}^{i,n}$ and l_{FP}^i are always taken as mesh points at the n-th iteration.

[2] Using η_m^n calculated in step [1], numerically integrating backwards the pressure equation (10) to obtain P^{n+1}, then from the variation of P^{n+1} determine the locations of PFZ-to-FFZ interfaces $l_{PF}^{i,n+1}$.

[3] Using η_s^n, η_m^n calculated in step [1] and $l_{PF}^{i,n+1}$ obtained in step [2], numerically integrating forward the heat equations (9) and (11) to obtain T^{n+1}.

Note that the mesh points used for numerical integration are designed similarly to the transient model.

Remark 3.1 In this paper, the degree of cook is modelled by the following reaction equation (Cai[1993]):

$$\frac{dg}{dt} = -k_g g^m, \tag{14}$$

where k_g is the rate constant, while $\mathcal{F} = 1 - g$ is the degree of cook.

The residence time distribution is modelled by the following dispersion equation (Levenspiel[1972]):

$$\frac{\partial C}{\partial t} + v\frac{\partial C}{\partial x} - D_a\frac{\partial^2 C}{\partial x^2} = 0, \tag{15}$$

where D_a is the dispersion coefficient, and v the average flow velocity.

4 MODEL VALIDATION

Unless measured values are available, the values of the parameters { K_d, B, a, C_m, C_s, U_m, U_s, η_m^0, n, δ, β, n_d, η_s^0, β_s, ρ, s }, used in the 1-D model, need to be estimated by non-linear regression. To validate the model, we have carried out parameter estimation by fitting the measurement data from 11 extruder runs with the following 15D high shear configuration:

5D feedscrew + 4 × 60° forward paddles + 2D feedscrew + 2 × 60° forward paddles + 2D single lead screw + 3 × 60° forward paddles + 3 × 60° reverse paddles + 0.25D orifice disc + 0.5D single lead screw + 4 × 30° reverse paddles + 1D single lead screw

Barrel temperature for each control zone i is set to: T_b(i)=T_0, i=0,1,...,4, $T_b(5)$=30°C, $T_b(6)$=60°C, $T_b(7)$=90°C, $T_b(8)$=120°C, $T_b(9)$=150°C.

Three different cases of feed rate with the same moisture content $M_0 = 0.20$ are investigated:
Case (a): $F_0 = 10kg/h$, **Case (b)**: $F_0 = 20kg/h$, **Case (c)**: $F_0 = 30kg/h$.

The estimated parameter values are all of reasonable magnitude. Tables 1-2 show the results of least-squares fitting of die pressure/temperature and zone 7/ zone 9 temperature. Figure 1 is the RTD fitting for the case of F=10 kg/h, N=300 rpm. The results of fitting are reasonably good except for a couple of exceptions.

Table 1

Case	N (rpm)	die pressure(MPa)			die temperature(°C)		
		num.	meas.	error	num.	meas.	error
(a)	200	2.448	2.717	9.9%	149.8	148.0	1.2%
	300	1.824	2.069	11.9%	151.7	147.5	2.8%
	350	1.610	1.848	12.9%	147.0	148.7	1.1%
	400	1.421	1.710	17.0%	148.9	149.0	0.1%
(b)	200	4.095	3.862	6.0%	150.6	148.0	1.8%
	300	2.953	2.883	2.4%	150.9	145.3	3.9%
	350	2.608	2.593	0.6%	151.0	147.6	2.3%
	400	2.333	2.393	2.5%	151.6	148.9	1.8%
(c)	200	5.558	5.683	2.2%	150.6	149.1	1.0%
	300	4.009	3.683	8.8%	150.9	149.0	1.3%
	350	3.539	3.414	3.6%	151.1	150.0	0.7%
	400	3.175	3.152	0.7%	151.3	151.0	0.2%

Table 2

Case	N (rpm)	melt temp. 7(°C)			melt temp. 9(°C)		
		num.	meas.	error	num.	meas.	error
(a)	200	76.5	77.0	0.6%	163.5	164.9	0.8%
	300	76.2	78.9	3.4%	170.6	171.5	0.5%
	350	78.2	79.0	1.0%	174.0	173.4	0.3%
	400	81.6	80.8	1.0%	177.3	174.0	1.9%
(b)	200	75.8	75.0	1.1%	162.8	162.5	0.2%
	300	74.0	75.0	1.3%	169.6	171.4	1.1%
	350	74.7	76.0	1.7%	172.9	175.4	1.4%
	400	76.6	76.0	0.8%	176.2	178.0	1.0%
(c)	200	75.7	73.0	3.7%	161.5	160.9	0.4%
	300	73.5	73.0	0.7%	167.8	165.4	1.5%
	350	73.9	73.2	1.0%	170.9	167.2	2.2%
	400	75.2	74.0	1.6%	174.0	176.7	1.5%

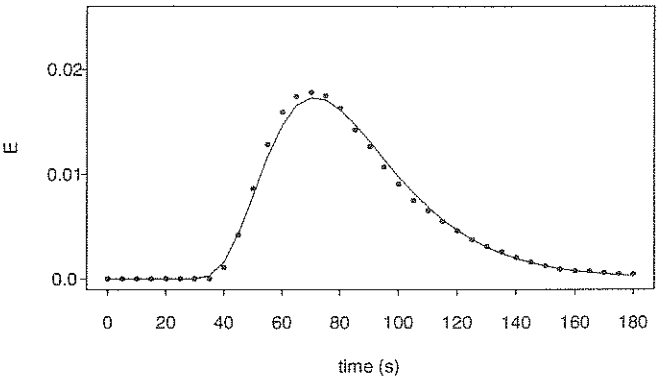

Figure 1: E-curve fitting for F=10kg/h, N=300rpm. "—"··· numer.; "•"··· experi.

5 CONCLUSION

The computer model discussed in this paper can simulate and predict extruder behavior (such as pressure, temperature, fill factor, gelatinization, residence time distribution, shaft power) under various operating conditions (such as feed rate, screw speed, feed temperature/moisture, barrel temperature) with reasonable good accuracy. It runs fast on a PC, taking only a fraction of a second to a few seconds. A graphic user interface (GUI) has also been developed, which makes this model user-friendly. Therefore, this model is suitable for designing and optimizing extruder operating conditions. Estimation of parameter values is, however, not easy. Further research addressing this problem is currently being undertaken.

6 ACKNOWLEDGEMENT

This work was carried out under the CSIRO priority project "*Smart Extrusion*", a joint project between CSIRO Division of Food Science and Technology and CSIRO Mathematical and Information Sciences. The author wishes to thank, in particular, Mr. Jay Sellahewa, Mr. Geoff Francis of CSIRO DFST and other staffs involved for conducting the extruder experiments for the purpose of model validation.

7 REFERENCES

Cai, W., and L.L. Diosady, Model for gelatinization of wheat starch in a twi-screw extruder, *Journal of Food Science*, 58(4), 872-875 and 887, 1993.

Chen, Z., and J.L. White, Simulation of non-isothermal flow in twin screw extrusion, *Inter. Polymer Processing*, IX(4), 310-318, 1994.

Frame, N.D., Operational characteristics of the co-rotating twin-screw extruder, in *The Technology of Extrusion Cooking*, edited by N.D. Frame, Chapter 1, Blackie Academic & Professional, 1994.

Kulshreshtha, M.K., C.A. Zaror, D.J. Jukes, and D.L. Pyle, A generalized steady state model for twin screw extruders, *Trans. IChemE*, 69(C), 189-199, 1991.

Kulshreshtha, M.K., and C.A. Zaror, An unsteady state model for twin screw extruders, *Trans. IChemE*, 70(C), 21-28, 1992.

Levenspiel, O., *Chemical Reaction Engineering*, 2nd ed., Wiley, New York, 1972.

Martelli, F.G., *Twin-Screw Extruders: A Basic Understanding*, Van Nostrand Reinhold Company, 1983.

Yacu, W.A., Modelling a twin screw co-rotating extruder, *Journal of Food Process Engineering*, 8, 1-21, 1985.

8 NOTATIONS

ρ — density;
η — apparent viscosity;
s — specific heat;
P — pressure;
T — temperature;
M — moisture content;
F — net forward mass flow rate;
$Q = \frac{F}{\rho}$ — net forward volumetric flow rate;
V_s — conveying volume per turn;
$F_f = V_s N \rho$ — conveying capacity;
$f = \frac{F}{F_f}$ — fill factor;
l_s — location of PFZ-to-FFZ interface;
L_b — barrel length;
V — volume of a C-shaped chamber;
V_p — volume of a twin-paddle section;
D — screw diameter;
D_e — equivalent twin screw diameter;
I — distance of two screw centers;
c_e — equivalent twin screw circumference;
ξ — pitch length;
e — axial length of a paddle or flight tip;
h — depth of screw channel;
θ — screw helix angle;
χ — flight clearance;
ϵ — gap between flight tip and channel bottom;
l_p — paddle tip width;
σ — gap between flight flanks of opposite screw.
d — die hole diameter;
K_d — die conductance;
N — screw speed;
K_o — orifice conductance.
n — power law index;
η^0 — coefficient of power law;
γ — shear rate;
δ — temperature coef. of viscosity;
β — moisture coef. of viscosity;
C — coef. of viscous heat generation;
U — heat transfer coef.;
B — coef. of pressure flow;
a — dimensionless constant;
ϕ — viscous heat generation factor.

Subscripts:
m — FFZ;
s — PFZ;
b — barrel;
d — die.

Note that $V_s = 2V$ for single lead screw, $V_s = 4V$ for double lead screw. For reverse screws, V_s is negative.